Authors' accepted manuscript. SAE Technical Paper, 2023. © SAE International
Final published version available at https://www.sae.org/publications/technical-papers/content/2023-01-1635/

2023-01-1635

Non-Evaporating Kerosene Fuel Spray Tip Penetration: A Comparison Between Phenomenological Models and Experiments

Pierre-Lou Billerot, Pascal Tétrault, Antoine Fleischmann, Romain Lemaire, Patrice Seers

École de Technologie Supérieure

Abstract

Interest in the use of kerosene fuel in diesel engines has garnered researchers' attention in the past few years due to its improve premixed combustion and its ability to decrease soot emission. The potential of using kerosene in the design stage of a diesel engine is thus a great motivator to study fuel spray development and to evaluate known fuel spray tip correlations and models with respect to their predictive capability with such a fuel. Therefore, the present paper proposes to investigate the spray development of a multi-hole solenoid injector fueled with kerosene under non-evaporative conditions. Moreover, the experimental results are used to evaluate how different phenomenological models proposed in the literature for diesel fuel are able to predict kerosene spray tip penetration. The experimental test rig is composed of a constant-volume pressurized vessel and a camera allowing to visualize the liquid phase using a backlight illumination technique. The influence of the injection pressure is studied at 400, 800 and 1600 bar, while three different injection durations (0.5, 1, and 2 ms) and five ambient pressures (2.5, 5, 10, 15 and 20 bar) are investigated. The experimental results are presented using a nondimensional time and fuel spray tip penetration to facilitate the analysis. The results show, as expected, that increasing the injection pressure or decreasing the ambient pressure results in a faster fuel spray tip penetration. The models that are evaluated include a constant ambient density hypothesis formulation, a variable ambient density model and three empirical correlations. A comparison between the models and experimental results shows that low injection pressure and short injection duration are two conditions in which the models have difficulty to predict the fuel spray tip penetration. Overall, the best performance was offered by the variable density model, which predicted the experimental data well.

Introduction

Interest in kerosene-based fuels in compression ignition engines has been increasing over the years. For example, an experimental study from Lee [1] showed that the use of kerosene (JP-8) improved the premixed combustion due to higher vaporization characteristics and a longer ignition delay than was the case using diesel. These properties lead to higher NO_x emissions than diesel, but are accompanied by lower levels of HC, CO and CO_2. The 2-color thermometry method was employed by [2] and confirms that local high temperature regions in the flame are responsible for the higher NO_x emissions from JP-8. Flame imaging also suggested a faster oxidation of JP-8 as compared to diesel, with the diffusion flame period in the former reduced, and consequently, the soot emissions as well.

Very often, kerosene is evaluated as part of a blend with other fuels. For example, Ashour et al. [3] investigated the addition of kerosene to diesel and biodiesel. They found that biodiesel B30 (30% biodiesel – 70% diesel fuel) blended with 15% of jet fuel was the most stable ternary blend, the latter allowing to achieve performances characterized by a coefficient of variation of IMEP less than 10%. This ternary fuel resulted in average CO and NO_x emission reductions of 53% and 14.3%, respectively, as compared to diesel. Similar trends were also reported by Patil et al. [4] with a 5 to 15% kerosene addition by volume to diesel. Elsharkawy et al. [5] compared the effect of blending up to 30% of castor biodiesel to diesel or kerosene at 2000 RPM and different loads. They found lower NO_x emissions at all loads with kerosene blends, and greater reductions with higher kerosene concentrations. For example, a 27.8% reduction of NO_x emissions was observed with a blended fuel composed of 90% kerosene and 10% castor oil, when compared to diesel, at a load of 40%. On the other hand, they found that CO emissions could be lower, higher or the same as with pure diesel fuel, depending on the engine loads for a same kerosene blend. Chen et al. [6] investigated a kerosene (RP-3)-pentanol blend (20% pentanol by volume), and reported a significant reduction of soot by an order of magnitude when compared to that of diesel at high load but without NO_x emissions increase [6]. However, CO increased by 39% and HC emissions were risen by a factor of 2.5 at low load, owing to the high latent heat of vaporization of pentanol, which led to lower in-cylinder temperatures.

While the preceding presents some advantages of using kerosene or kerosene blend fuel in diesel engines, few studies have investigated its fuel spray development. In one investigation, Yu et al. [7] compared the spray characteristics of diesel and kerosene using diesel injectors, and showed that under the same injection conditions, diesel and kerosene offer a similar momentum flux at the nozzle outlet during the steady-state phase of the injection process. However, they also reported a slower needle closing at the end of the injection with kerosene. Overall, a slightly lower spray tip penetration was observed, and was attributed to a lower fuel viscosity and increased nozzle cavitation [7]. Song et al. [8] investigated fuel spray development of ethanol-kerosene fuel blends with up to 30% ethanol. They reported very little difference between kerosene and ethanol-kerosene blends with respect to fuel spray tip penetration.

In general, diesel fuel spray is experimentally characterized due to its importance on the ensuing mixture formation and combustion

processes. One of the important characteristics of the fuel spray is its tip penetration as it quantifies the contact between fuel and the surrounding air. Fuel spray tip penetration is also an important parameter because wall impingement with the combustion chamber bowl is to be minimized. Therefore, during the design process, and due to its low computational cost, a phenomenological model can be used to study different combustion chamber configurations or to perform parametric studies [9]. Some of the phenomenological models or correlations found in the literature used a constant injection pressure (P_{inj}), such as in Naber et al. [10], while others used a variable P_{inj} or fuel spray momentum as input [11, 12]. Of course, phenomenological models have some limitations in their ability to predict the fuel spray tip penetration [9]. For example, most models are more accurate in the fully developed region (far from the nozzle) of the spray. Other models, such as that initially proposed by Hiroyasu et al. [13], and which covers near-nozzle penetration and the fully developed region, have been adapted or improved over the years. Yet, others, such as the one proposed by Roisman et al. [14], considered the compressibility effect of the gas in the early spray development phase. While the shortcomings of phenomenological (or semi-empirical) models have been identified, these modeling approaches continue to be proposed or to be validated for a wider range of data due to their advantages in the early phase of the design process.

As interest in kerosene fuel applied to the diesel engine continues to soar, fuel spray tip penetration must be quantified, given its thermophysical properties, which are different from those of conventional diesel. Moreover, because spray tip penetration is so crucial in the early phase of the design process, it is proposed to compare different phenomenological models in terms of their ability to predict the phenomenon. Multiple-injection strategies are widely used in diesel engines, which is why three injection durations (or energizing times, ET) are evaluated, and notably cover a short injection, allowing evaluating the models' performance under these conditions.

Therefore, the present study first aims at measuring fuel spray tip penetration of a multi-hole injector fed with kerosene. Second, based on the experimental results obtained under various injection conditions in non-evaporative environments, five models from the literature are compared with respect to their ability to predict fuel spray tip penetration.

Experimental Set-Up and Methodology

Experimental Apparatus

Fuel Spray Visualization

The experimental set-up used for non-evaporative experiments is shown in Figure 1, and consists of a 6.1 L constant-volume pressurized vessel with four optic ports having sapphire windows that allow an 8 cm field of view. A Haskel DSHF-300 pneumatic high-pressure fuel pump fed the injector fuel rail with kerosene. The thermophysical properties of the kerosene fuel used in this study are reported in Table 1.

Table 1. Thermophysical properties of kerosene fuel [15]

Density at 298K (kg/m^3)	~790
Viscosity at 303K (mPa-s)	1.2

The fuel rail pressure was adjusted by regulating the pump's air supply pressure, while the fuel rail pressure was monitored using the Bosch pressure sensor mounted on the fuel rail. The injection unit is a multi-hole solenoid-actuated injector from the Bosch CRI2 series, a widely used injector in light-duty Diesel direct injection engines [16]. The vessel was pressurized with nitrogen and the pressure was monitored with a Sensotec TJE/1035-26 pressure transducer. Once the desired ambient pressure (P_{amb}) was reached, an Omega SV120 valve closed. Signal acquisition and control of the injector and camera were done using a second interface and a CompactRIO NI-9074. When the set P_{amb} was reached, a NI-9751 injection module generated a typical current profile and the injection started. Simultaneously, a TTL signal generated by the NI-9401 module triggered the camera to start recording. The camera (model Phantom VEO410L) was equipped with a Nikon 50 mm f/1.4 Nikkor AF-D objective and a back-illumination technique is used. The acquisition frame rate was set to 57000 fps, with a resolution of 256×256 px^2. The videos were recorded in PCC 3.4 for subsequent post-processing.

Image Processing Method

The post-processing of the liquid fuel images is based on a 4-step process proposed by Jourdain et al. [17] for micro- and macroscopic spray analysis. First, a background image is taken just before the spray appears, and is removed from all spray images. Second, the background-removed image is filtered using a multi-scale Bayesian filter [18]. Third, the filtered image is post-processed using the contour detection method proposed by Chan et al. [19]. Finally, the image is binarized, allowing to determine the position of the spray tip. The liquid penetration length is based on a jet that is perpendicular to the field of view. It should be noted that the spray development in the first images (approximately the first 5 mm) is not reported because it cannot be properly illuminated from the back, making any post-processing difficult or unreliable. The missing data in the initial penetration profile thus corresponds to this effect.

Instantaneous Mass Flow Rate

The instantaneous mass flow rate was measured using an in-house long tube method apparatus similarly to [20]. The method is based on the measurement of the appearance of a pressure wave due to the injection process, which is recorded using a piezoresistive pressure sensor (Kistler 6061) and a charge amplifier (Kistler 5010a). The equipment (fuel pump, CompactRIO chassis) used to pressurize the fuel and to control the injector during the spray visualization was also used for the instantaneous mass flow rate measurements. The CompactRIO chassis includes a 16-bit acquisition card (NI-9222) that enabled acquiring the pressure signal at a 250 kHz sample rate. From the dynamic pressure measurement ($P(t)$), the instantaneous mass flow rate ($\dot{m}(t)$) was obtained using Equation (1), where $\mathcal{A}$ is the tube cross-section area and c is the speed of sound in the fuel. For each test condition, experiments were repeated 25 times, allowing to obtain an average instantaneous mass flow rate. The coefficient of variation on the total mass injected over the 25 samples was found to be between 4.2% (at 800 bar) to 4.5% (at 1600 bar).

$$\dot{m}(t) = \frac{\mathcal{A}}{c} \cdot P(t) \tag{1}$$

Data post-processing of the pressure signal was performed using MATLAB® with an in-house code. Because the raw pressure signal is inherently noisy [21], the signal was thus filtered using a Butterworth filter with a third-order cut-off set at 21.25 kHz to minimize its impact

on the signal and to remove high frequency noise. Overall, the method used herein is similar to that of Menucci [22].

As will be shown in the modeling section, the momentum flux of the spray is required as an input to some models. Therefore, the instantaneous mass flow rate is used to compute the instantaneous fuel jet momentum using Equation (2) [23].

$$\dot{M}_0(t) = \frac{\left(\frac{\dot{m}(t)}{n_h}\right)^2}{\rho_f \cdot \pi \cdot \frac{d_n^2}{4}} \tag{2}$$

where n_h denotes the number of holes, ρ_f is the fuel density, and d_n is the injection nozzle diameter.

Test Conditions

The non-evaporative test conditions covered herein are presented in Table 2, where for each ET, three different P_{inj} and five P_{amb} have been tested. Note that the ambient temperature is kept constant at 298 K. As can be observed in Table 2, a short injection duration of 0.5 ms is evaluated as representative of the ET duration in multiple-injection strategies, which are widely adopted to reduce in-cylinder NO_x, foster soot oxidation and decrease combustion noise [24]. Overall, 15 different test conditions per ET were executed. A variability study was performed and revealed that a total of four tests are needed to keep the mean coefficient of variation of the penetration below 7%. Data outliers were discarded using the Pierce's criterion [25] in order to calculate representative mean penetration profiles that will be used in the comparison with phenomenological models.

Table 2. Test conditions

Injection duration ET (ms)	Injection pressure P_{inj}	Ambient pressure P_{amb} (bar)
0.5, 1 and 2	400, 800 and 1600	2.5
		5
		10
		15
		20

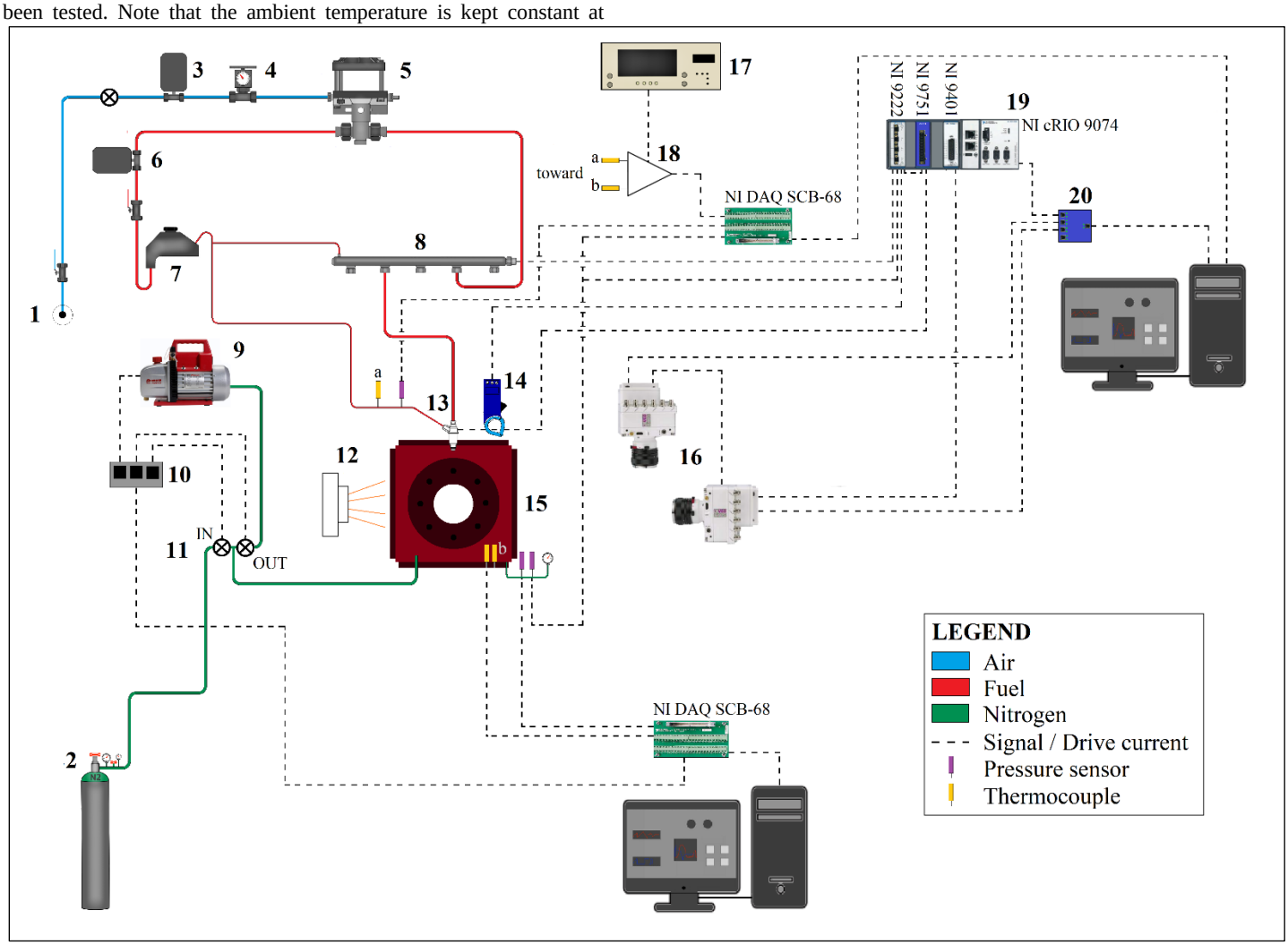

Figure 1. Experimental set-up: 1. Compressed air; 2. Nitrogen-pressurized bottle; 3. Air filter; 4. Fuel pump air pressure adjusting valve; 5. High-pressure fuel pump; 6. Fuel filter; 7. Fuel reservoir; 8. Fuel common-rail; 9. Vacuum pump; 10. Relays; 11. Filling and emptying valves; 12. Light source; 13. Fuel injector; 14. High-current probe; 15. Pressurized vessel; 16. High-speed cameras; 17. Voltage generator; 18. Thermocouple amplifier; 19. CompactRIO; 20. Network Switch

Results

The beginning of the injection is characterized by an almost linear relationship between time and penetration. This period is associated with the acceleration of the spray tip until it reaches its maximum velocity [26]. This quasi-linear region located near the nozzle exit is then followed by the fully developed region, where a change of slope and the evolution of the penetration is no longer linear due to the spray tip deceleration. The inflexion point between both regions corresponds to the breakup timing (t_b), where the uniform liquid core formed by the jet is atomized in small droplets. Recently, Arai [27] proposed a nondimensional time (t^*) and fuel spray tip penetration (S^*) based on the liquid spray breakup length (L_b). According to this 'breakup scaling' [27], $S^* = t^*$ for ($t^* \leq 1$) while $S^* = \sqrt{t^*}$ for a time above the breakup time ($t^* > 1$). The nondimensional time and penetration are defined in Equations (3) and (4) with respect to t_b and L_b, respectively, as follows [27]:

$$t^* = \frac{t}{t_b} = \frac{(\rho_{amb} \cdot \Delta P)^{1/2}}{K_{bt} \cdot \rho_f \cdot d_n} \cdot t \tag{3}$$

$$S^*(t) = \frac{S(t)}{L_b} = \frac{\sqrt{\rho_{amb}}}{K_{bl} \cdot \sqrt{\rho_f} \cdot d_n} \cdot S(t) \tag{4}$$

In these equations, K_{bt} and K_{bl} are constants with values ranging from 8.84 to 28.7 for the former, and from 10 to 15.8 for the latter, when diesel fuel is used, depending on the kind of diesel injector [27]. The estimation of K_{bt} implicitly considers the viscosity and surface tension of the fuel. Furthermore, the liquid viscosity impacts the injection velocity, which is dependent on K_{bl}. Thus, because kerosene is used herein, both variables need to be adjusted in this study. To this end, all the data for each P_{inj} was used to find K_{bt} and K_{bl} that minimize the difference with the experimental data using a least square method in MATLAB® (*lsqcurvefit* function). The three values obtained for each constant were then averaged and the resulting K_{bt} and K_{bl} were used without any further modification. This approach was used to first see if there was a difference between each P_{inj} and it was observed that for an injection pressure of 400 bar, the values differ from those of the two others P_{inj}. This difference might be linked to the dynamic of the injector as the needle displacement is dependent on the injection pressure. Thus, the lower P_{inj} provides a much slower needle motion, while it is assumed that the difference in needle motion between the higher P_{inj} is less significant, resulting in a similar value for each constant. Considering that K_{bt} and K_{bl} are linked to the discharge coefficient (K_v) of the nozzle, K_v was computed using the spray tip penetration data as a function of time as per [27] such that $U_{spray} = \frac{dS}{dt} = K_v \cdot \sqrt{\frac{2\Delta P}{\rho_f}}$ in the linear spray region. It was found that K_v is about 30% lower for the lowest P_{inj} when compared to the other P_{inj}, which were found to be similar. For kerosene and the injector considered herein, the average values are $K_{bt} = 98.4$ and $K_{bl} = 26.9$, which is consistent with a fuel having a lower viscosity than diesel fuel, based on [27]. The different values associated with this non-dimensional approach are presented in Table 5. Finally, this approach was chosen herein to help analyze the results as it allows to graphically more easily highlight some differences with the conventional dimensional spray tip penetration as a function of the time approach.

Effect of Injection Pressure

The influence of P_{inj} at a constant P_{amb} and ET is shown in Figure 2, which also displays the theoretical linear and fully developed S^* behaviors. Three injection pressures are presented, namely, 400, 800 and 1600 bar. Moreover, as P_{inj} increases, the injector opening delay decreases, and this effect was taken into consideration by shifting the curves accordingly in order to provide a spray tip penetration that begins at time zero for all P_{inj}.

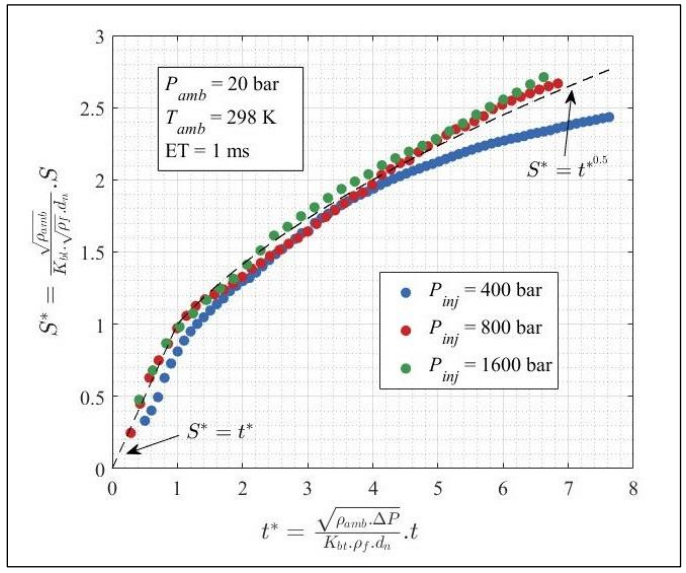

Figure 2. Influence of injection pressure
($P_{amb} = 20$ bar; $T_{amb} = 298$ K; ET = 1 ms)

Figure 2 shows that for a P_{inj} of 800 and 1600 bar, the spray tip penetration follows rather well the linear phase of the spray, while the data for a P_{inj} of 400 bar suggests an early non-linear behavior for $t^* < 0.5$, which is less visible for the higher pressure, but is nonetheless still present. This result is in concordance with the early fuel tip penetration of Li et al. [26], who reported that the early region of the spray, under non-evaporative conditions, follows a relationship in which $S(t)$ is proportional to $t^{1.566}$. Herein, the exponent is not as strong. In the fully developed region ($t^* \geq 1$), the sprays of Figure 2 also follow rather well the general relationship of Arai [27], with $S^* = t^{*0.5}$ for the highest P_{inj}. For the lowest injection pressure and for t^* above approximately 4.5, the general trend of the fuel tip penetration does not follow the $S^* = t^{*0.5}$ relationship owing to a greater deceleration rate of the spray penetration due to a greater momentum dispersion in the spray tip [27]. This behavior appears at a time that is about twice the injection duration, which was also observed by Zhou et al. [28], who used it as a condition for their model development that will be shown later.

Effect of Ambient Pressure

Figure 3 shows the influence of the ambient pressure for five different P_{amb} (2.5; 5; 10; 15 and 20 bar). ET and P_{inj} are kept constant at 1 ms and 1600 bar, respectively. It has been reported that in the near region of the injection ($S(t)$ vs. time, thus dimensional penetration), the effect of the P_{amb} is negligible as the curves are superimposed [26]. However, because the non-dimensional approach is used, the results show a higher slope for the linear part of the spray for $P_{amb} \leq 5$ bar. They also show that the linear behavior lasts for nearly the entire field

of view of the pressurized vessel used herein for these particular cases. At this high P_{inj}, the penetration is controlled by the spray momentum due to the high spray velocity at the nozzle exit. Then, it is observed that an increase of the ambient pressure results in a decrease of the rate of linear penetration. Indeed, with increasing P_{amb}, a higher gas density causes a greater resistance to the spray. Thus, the fuel spray experiences a higher aerodynamic drag and penetrates more slowly [29]. Figure 3 shows that the fully developed region follows rather well the general trend $S^* = t^{*0.5}$ for the highest P_{amb}. Similar results were obtained with a P_{inj} of 800 bar. With a P_{inj} of 400 bar, a few differences were observed. First, for a P_{amb} of 20 bar, the data fall below the straight line in the linear region of the spray, as can be seen in Figure 2. Second, after a time t^* approximately equal to twice the nondimensional ET, the curves for a P_{amb} of 15 and 20 bar do not follow $S^* = t^{*0.5}$ due to a greater deceleration, similarly to what was observed in the previous section.

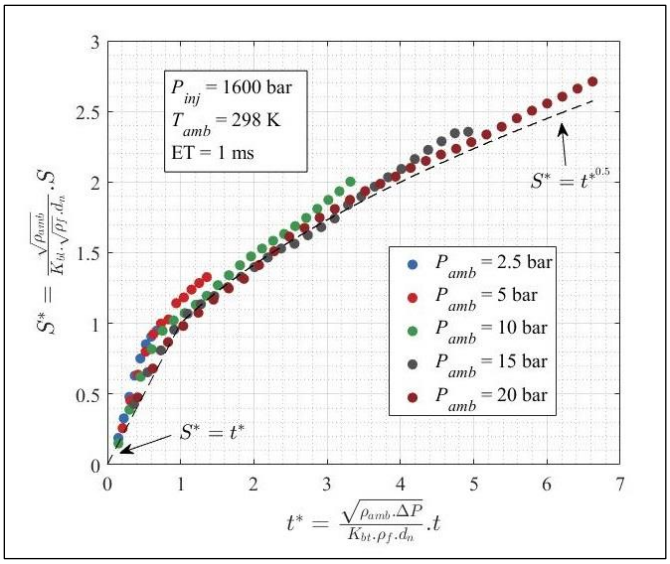

Figure 3. Influence of ambient pressure
(P_{inj} = 1600 bar; T_{amb} = 298 K; ET = 1 ms)

Effect of Injection Duration

The impact of the injection duration is presented in Figure 4 for a P_{inj} of 800 bar and a P_{amb} of 15 bar. The results show a similar behavior for the linear part of the spray for all three injection durations. However, the shorter injection duration (ET = 0.5 ms) shows a deviation of the trend $S^* = t^{*0.5}$ in the fully developed region approximately at a t^* of about 3. The beginning of the deviation corresponds once again approximately to a time twice as long as the injection duration, as was also observed in Figure 2 for the lower P_{inj}. Following this time, the exponent n is decreasing in the relationship $S^* = t^{*n}$ due to increasing fuel spray tip momentum loss. For the two other injection durations, the maximum t^* shown in Figure 4 is less than twice the respective ETs.

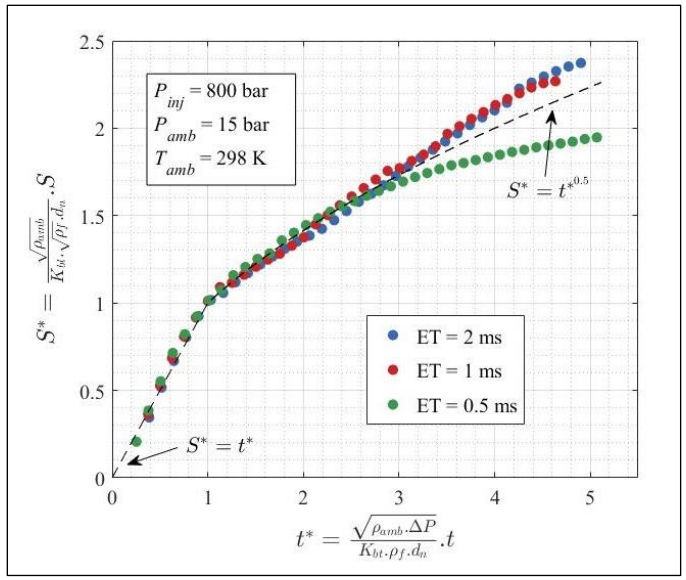

Figure 4. Influence of ambient pressure
(P_{inj} = 800 bar; P_{amb} = 15 bar; T_{amb} = 298 K)

Fuel Spray Penetration Modeling

The modeling of the spray penetration under non-evaporative conditions was undertaken using different approaches, which are briefly presented in the next sections. First, constant and variable ambient density models from the literature are presented, based on the instantaneous fuel momentum flux, to determine the spray tip penetration. Second, three correlations from the literature, based on a constant injection pressure, have been identified and are briefly presented.

Constant Density Model

The constant density model was developed in [11, 30] for the fully developed region of the spray. It is based on the momentum flux conservation along the spray axis. The momentum flux from the spray exiting the nozzle can be computed based on the instantaneous mass flow rate measurements which were measured herein as described above. The hypothesis in the constant density model is that the fuel jet velocity and momentum flux are replaced by a gas jet with the same properties. To this end, and to compensate for the difference in density, an equivalent diameter (d_{equiv}) to the nozzle is defined as per Equation (5) [30]:

$$d_{equiv} = d_n \cdot \left(\frac{\rho_f}{\rho_{amb}}\right)^{1/2} \tag{5}$$

Non-stationary conditions are considered by dividing the momentum flux profile into individual packets sequentially injected as proposed in [11]. The momentum flux of a given packet is the sum of its own momentum flux and the momentum of the packet that directly precedes it because the packet is injected in an environment that is already disturbed, except for the first packet. Then, the penetration of the ith packet is derived from the momentum conservation law along the spray axis, assuming a constant ambient density, a Gaussian radial velocity profile in the spray, and the concept of isodensity jet, as major hypotheses. This leads to Equation (6) [30]:

$$S_i(t) = \left(\frac{2 \cdot \alpha}{\pi}\right)^{0.25} \cdot \frac{2}{K_u} \cdot \dot{M}_i^{\,0.25} \cdot \rho_{amb}^{\,-0.25} \cdot \tan^{-0.5}\left(\frac{\theta}{2}\right) \cdot \sqrt{t_i'} \tag{6}$$

where α is the Gaussian shape factor (value equal to 4.605 [30]), K_u (value equal to 1.980 [30]) is a constant of proportionality between the spray axis velocity and the spray tip velocity, and θ is the spray cone angle. Herein, θ is estimated using the correlation presented in [10]. t_i' is the scaled time after the injection of the ith packet. Eventually, any packet will reach the spray tip and become the leading packet in the spray. To ensure the continuity of the global penetration formed by the penetration of the successive leading packets, a phase shift introduced in t_i' is calculated for each packet. Finally, the global penetration corresponds to the penetration of the most forward packet.

The model was coded in MATLAB® and a simulation based on the experimental data of the momentum flux of [11] was used to validate the numerical implementation. The results of the simulation are presented in Figure 4, allowing a comparison with the experimental results of the original authors of the model. The very good concordance between the numerical implementation herein and the results of [11] with respect to the fuel spray tip penetration thus confirms a proper numerical implementation.

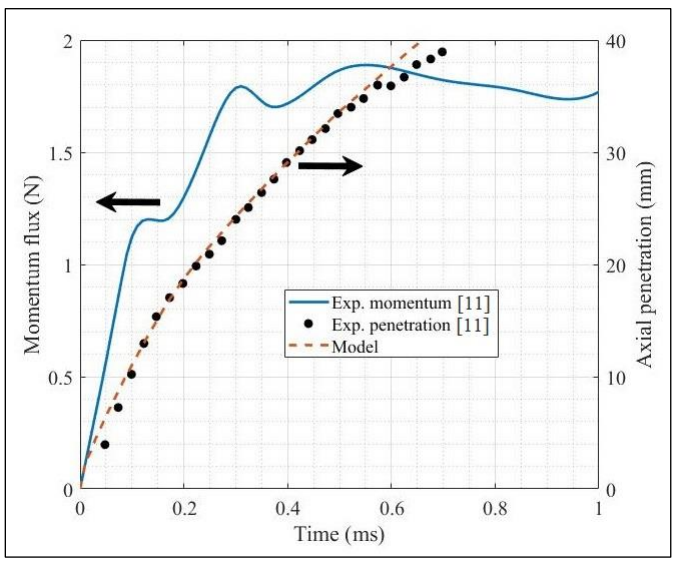

Figure 4. Validation of the spray tip penetration of the constant density fuel spray tip model

Variable Density Model

Unlike the previous approach, the model developed by Katrašnik [12], and briefly presented herein, assumes a jet density different from the ambient density. Note that the spray density is variable in time but constant in space. Moreover, this model is able to predict the position of the spray tail and the fuel concentration within the spray, assuming a Gaussian profile around the centerline. The equation for the spray tip penetration is given by Equation (7) [12]:

$$S(t) = \sqrt{S_{tail}^2(t) + \frac{\sqrt{\widetilde{M}_0} \cdot t}{\sqrt{\frac{\pi \cdot \rho}{2\alpha}} \cdot \tan\left(\frac{\theta}{2}\right) \cdot (1 - e^{-\alpha})}} \tag{7}$$

where $S_{tail}^2(t)$ is the position of the spray tail, which is attached to the spray nozzle while the injection process is ongoing, but will vary with time after the end of injection. $\widetilde{M}_0$ is the time-averaged momentum flux obtained as per Equation (8):

$$\widetilde{M}_0 = \frac{\int_0^t \dot{M}_0 dt}{t} = \frac{M_0}{t} \tag{8}$$

The instantaneous momentum flux $\dot{M}_0$ is estimated from Equation (2). The value of the spray density involved in Equation (7) is computed at each time step of the injection using Equation (9), in which m_f is the mass of fuel obtained by integrating the mass flow rate, m_{jet} is the spray total mass and $\rho_{f,vap}$ is the density of the fuel vapor.

$$\rho = \frac{\rho_{amb}}{1 - \frac{m_f}{m_{jet}}\left(1 - \frac{\rho_{amb}}{\rho_{f,vap}}\right)} \tag{9}$$

In this paper, the use of the model is restricted to the prediction of the spray tip penetration, but additional details about the spray tail penetration and the fuel distribution can be found in [12].

Following the same procedure as before, the model is coded in MATLAB®, and a simulation is run based on the input parameter presented in [12]. This allows comparing the spray tip penetration with the results presented in [12] and to validate the numerical implementation of the model. The results are presented in Figure 5, where a very good concordance is observed between both numerical results.

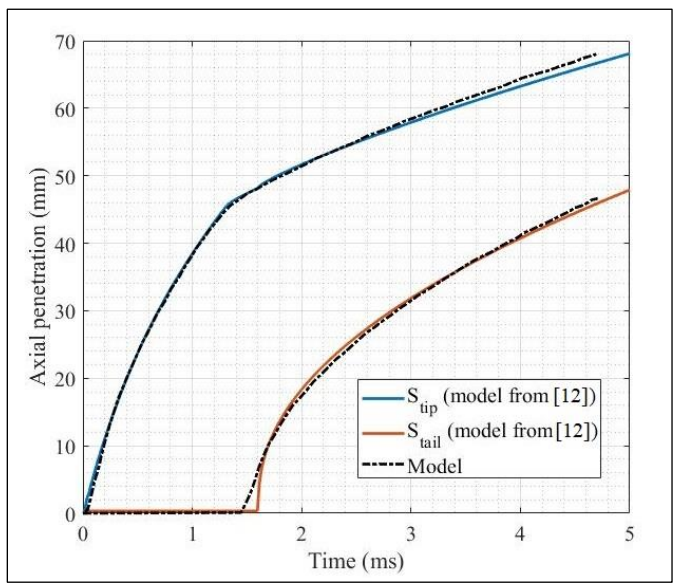

Figure 5. Validation of the spray tip penetration of the variable density fuel spray tip model

Correlations

Simpler correlations were chosen to evaluate their behavior in predicting the fuel spray tip penetration while having different hypotheses leading to their respective equations.

Model of Roisman et al.

The first correlation evaluated was proposed by Roisman et al. [14], and is valid in the diluted region of the spray, where the fuel jet is considered steady. The distance from the nozzle at which the spray begins to be considered diluted is given by a breakup length. Based on the results presented in [14], this breakup length, which represents the distance R_0 from the nozzle outlet, is given by a correlation presented by Equation (10). In this equation, the constant value 2.5 is a function of the injector and of the liquid properties, and its value is associated to diesel. As reported in [14], a constant value of 15.8 has been obtained for water in a previous publication.

$$R_0 = 2.5 \cdot d_n \cdot \left(\frac{\rho_f}{\rho_{amb}}\right)^{1/2} \tag{10}$$

When this condition is met, the ambient air is considered as incompressible and the spray tip penetration is given as a function of the ambient conditions and injector nozzle diameter as per Equation (11):

$$S(t) = \left[a + \frac{\left(2-\sqrt{2}\right)^{1/2} \cdot \left(2+\frac{2 \cdot \rho_{amb}}{0.311 \cdot \Delta\rho}\right)^{1/2} \cdot \left(\frac{d_n}{c}+\tau\right)^{1/2}}{\left(\frac{\rho_{amb} \cdot (0.311 \cdot \Delta\rho + \rho_{amb})}{0.311^2 \cdot \Delta\rho^2}\right)^{1/4}}\right] \tag{11}$$

In Equation (11), a and τ are two model constants that are adjusted to fit with the experimental data as a function of P_{inj}. Their values were obtained using a least square method (*lsqcurvefit* function) available in MATLAB®, and the end results for each P_{inj} are shown in Table 4. The data were fitted to a higher P_{inj} than initially proposed by the authors in [14], who validated their model for P_{inj} between 300 and 1350 bar and for P_{amb} between 1 and 25 bar. For the initial prediction of the fuel spray up to the breakup length, defined by Equation (10), Roisman et al. [14] proposed a different approach that considers the gas compressibility. For the test conditions herein, R_0 has a value between 3 and 8 mm, and because the first 5 mm of spray is very difficult to detect with the experimental set-up, the initial fuel spray tip equations of Roisman et al. [14] are not considered herein.

Table 4. Fitted coefficients of Equation (11)

Injection pressure P_{inj} (bar)	Coefficients of Equation (11)
400	$a = -0.0289$ $\tau = 3.055e-5$
800	$a = -0.0145$ $\tau = 1.546e-5$
1600	$a = 0.0027$ $\tau = -2.894e-5$

Improved model of Hiroyasu and Arai

The second set of correlations evaluated herein were initially proposed for long injection durations by Hiroyasu et al. [13] (Equations (12) to (14)), with a P_{inj} of 1500 bar and a P_{amb} between 5 and 40 bar. The original correlations of [13] make a distinction between two equations by using a breakup time (t_b) defined as per Equation (12):

$$t_b = K_{bt} \cdot \frac{\rho_f \cdot d_n}{\sqrt{\rho_{amb} \cdot \left(P_{inj} - P_{amb}\right)}} \tag{12}$$

Hence, in the early phase of the injection process, when $0 < t \leq t_b$, the fuel spray tip penetration is considered to be proportional to time and the fuel spray momentum is constant. This first phase of the spray tip penetration is given as follows:

$$S(t) = K_v \cdot \left(\frac{2 \cdot \left(P_{inj} - P_{amb}\right)}{\rho_f}\right)^{1/2} \cdot t \tag{13}$$

While, after t_b, the spray tip penetration enters a period defined as a transition phase during which the momentum decreases, during this second phase, $S(t)$ is provided by Equation (14).

$$S(t) = K_p \cdot \left(\frac{\left(P_{inj} - P_{amb}\right)}{\rho_{amb}}\right)^{1/4} \cdot d_n^{1/2} \cdot t^{1/2} \tag{14}$$

Finally, the last model evaluated in this work was proposed by Zhou et al. [28], who improved the above correlations by considering the spray development after the end of injection, which is of interest when a short injection strategy is used. For this particular case, a deceleration phase of the spray is defined after a period equal to twice the injection duration ($t > 2 \cdot \mathrm{ET}$). Hence, Zhou et al. [28] proposed using Equation (13) when $t \leq t_b$, while using Equation (14) for $t_b < t < 2 \cdot \mathrm{ET}$. Then, once $t > 2 \cdot \mathrm{ET}$, Equation (15) was used and was proposed to ensure continuity with Equation (14) at $t = 2 \cdot \mathrm{ET}$:

$$S(t) = \sqrt{2} \cdot K_p \left(\frac{\left(P_{inj} - P_{amb}\right)}{\rho_{amb}}\right)^{1/4} \cdot d_n^{1/2} \cdot \mathrm{ET}^{1/4} \cdot (t - \mathrm{ET})^{1/4} \tag{15}$$

The above equations were evaluated by [28] using a short ET of 0.6 ms in combination with a P_{inj} between 900 and 1800 bar, a P_{amb} of 13.1, 17.5 and 21.8 bar, at a constant temperature of 293 K. In their analysis, the authors reported a better fit between the experimental data and Equation (13) if the relationship with respect to time is at power 1.4 ($t^{1.4}$). The values associated with the coefficients of Equations (12) to (15) are shown in Table 5, and illustrate the impact of using kerosene.

Table 5. Coefficients in empirical correlations

Coefficient	Original value [13] with diesel fuel	Value in this work with kerosene
K_{bt}	28.65	98.4
K_{bl}	15.8	26.9
$K_v = \frac{K_{bl}}{\sqrt{2} \cdot K_{bt}}$	0.39	0.19
$K_p = 2^{0.25} \cdot \sqrt{K_{bl} \cdot K_v}$	2.95	2.71

Comparison of the Models with Experimental Measurements

A comparison between the models and experimental results was conducted with different ET. Thus, at a low P_{inj} of 400 bar, only a long injection of 2 ms was compared, while a 1 and 2 ms injection were shown when P_{inj} was set at 800 bar. Finally, the performance of the above equations was evaluated at P_{inj} of 1600 bar with ET of 0.5, 1, and 2 ms.

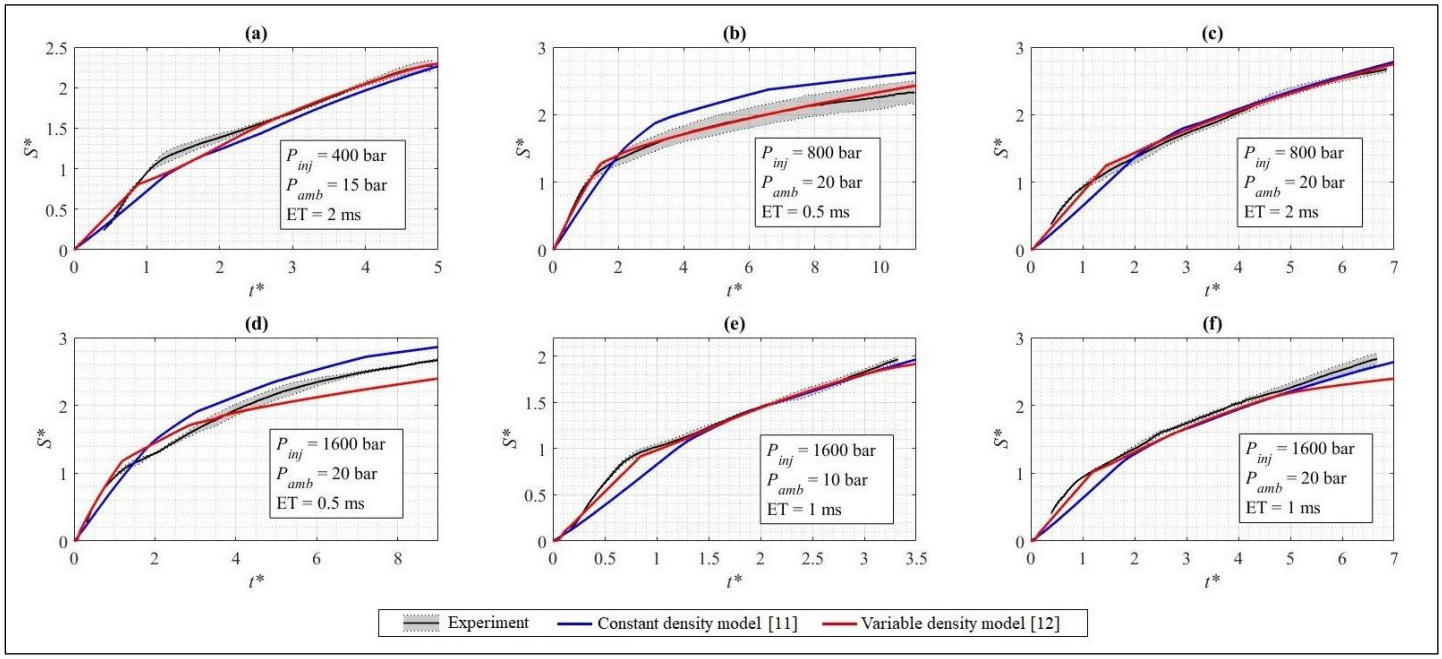

Figure 6. Comparison of the constant and variable density models' predictions with experimental measurements

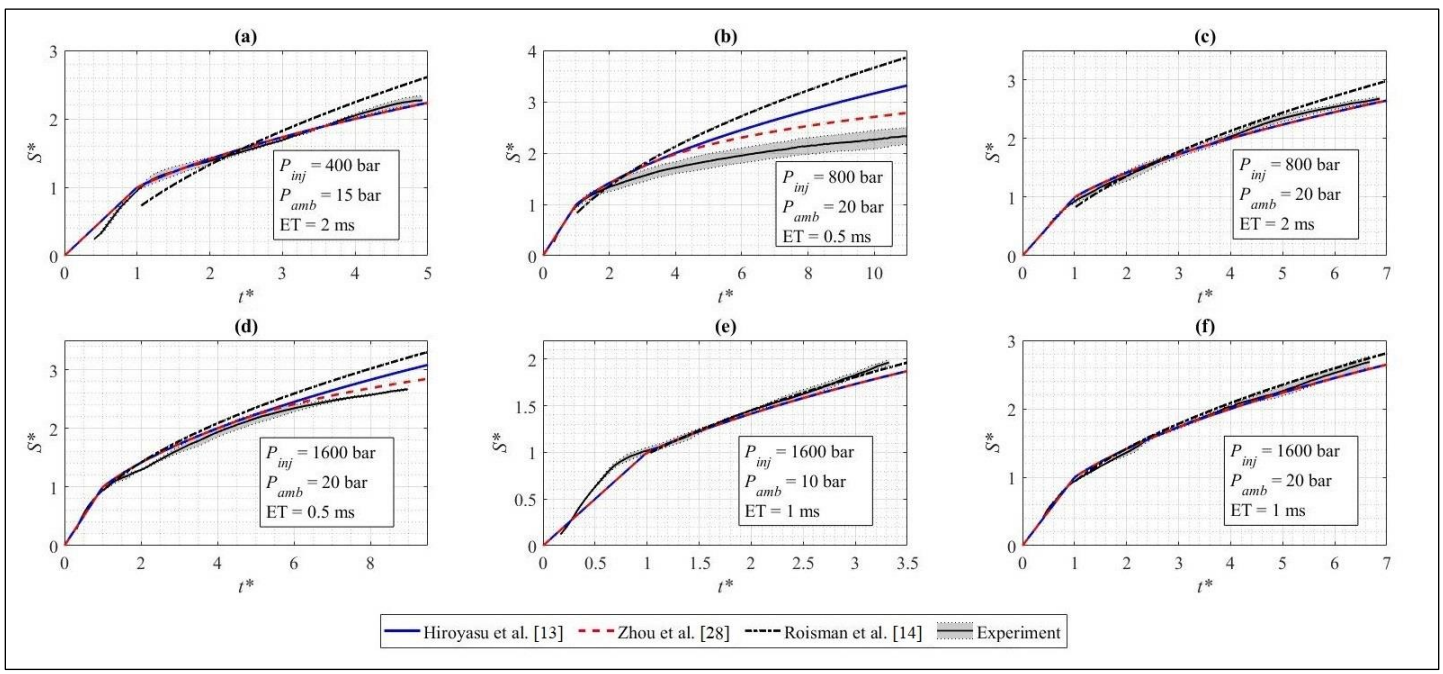

Figure 7. Comparison of the predictions obtained with correlation against experimental measurements

Figure 6 compares the more complex models of Payri et al. [11] and Katrašnik [12] against different experimental fuel spray tip penetrations representing the spectrum of conditions tested herein. Both models use the instantaneous momentum flux measured experimentally as an input. Figure 6 (a) illustrates the difficulty of correctly predicting the early phase of the injection process at a low P_{inj} even if ET lasts 2 ms. Once the fully developed region is well established, both models correctly predict the last half of the spray tip penetration, with an overall better performance with the variable density model. Figure 6 (b) presents both model behaviors for a short ET of 0.5 ms, a P_{amb} of 20 bar and a P_{inj} of 800 bar. This short injection is really well reproduced by the variable density model during the linear and fully developed phases of the spray, while the constant density model shows an underprediction for the linear part of the spray and an overprediction afterward, as also observed by others [31]. The effect of increasing the injection duration is shown in Figure 6 (c), where an improvement in the fully developed region of the spray tip penetration is observed with the constant density model with respect to the short injection. The variable density model still performs very well. Finally, at a high P_{inj} of 1600 bar, Figure 6 (d-f) shows the impact of varying ET at a constant P_{amb} (Figure 6 (d) vs. (f)), while the effect of P_{amb} at a constant ET is compared with Figure 6 (e) and

(f). Again, the variable density model offers a better overall prediction, with a proper representation of the early part of the spray even for the short ET for which the fully developed phase is underpredicted by the variable density model and overpredicted by the constant density model. For longer ET, the quality of the prediction improves in the fully developed region for both models. Overall, the variable density model offers a very good capability to predict the different conditions tested herein.

The same approach is used to compare the above correlation models, acknowledging that the model proposed by Roisman et al. [14] needs to have two model constants set based on the experimental data. Therefore, a good match is thus expected, a priori, for such an approach. However, it appears that calibrating such a model for a given P_{inj} using multiple ET and P_{amb} does not guarantee a successful prediction as the model constants are very sensitive to all the variables at play. The results can be seen in Figure 7 (a), for a P_{inj} of 400 bar with an ET of 2 ms, where the model intersects the experimental data in the fully developed region. A similar response from the model is also obtained at a P_{inj} of 800 bar (see Figure 7 (b)) in combination with a short ET of 0.5 ms. Overall, the curve fitting approach does not allow a good match unless the highest P_{inj} is used.

The correlation proposed by Hiroyasu et al. [13] allows a better fit of the spray tip penetration with respect to the experimental trend observed, and is simpler to use. At a P_{inj} of 400 and 800 bar, and for a long ET of 2 ms, the fully developed part of the spray is well reproduced by the approach of Hiroyasu et al. [13], as can be observed in Figure 7 ((a) and (c)), while an overprediction is observed for a short injection as expected (Figure 7 (b)). The modification proposed by Zhou et al. [28] for a short injection can be seen in Figure 7 (b), and allows a slight improvement with respect to the trend of the spray tip. Finally, at the highest P_{inj} (see Figure 7 (d) to (f)), all three correlations behave similarly, with a slight over-prediction for the fully developed part of the spray with the shortest ET.

Overall, it is observed that all models offer a better prediction of the spray tip penetration under a long ET and high P_{inj} because one common hypothesis in the proposed equations is that the models are applied to the diluted or fully developed region of the spray. When short injections are considered, the time for the needle transient displacement is not negligible with respect to the total injection duration and thus impacts the spray tip penetration. This transient needle displacement is characterized by a throttling effect on the flow within the injector while a low P_{inj} increases the transient needle displacement duration due to a slower needle speed [32]. Furthermore, during the transient needle displacement, it is assumed that the fuel pressure at the nozzle inlet is lower than P_{inj}, but increases with the needle displacement until the steady-state flow regime is reached as in the conceptual model of Zhou et al. [33]. When considering the influence of using a low P_{inj} (for a given ambient pressure), it has been shown experimentally that it increases the time and distance for the fuel spray tip to reach its steady-state regime due to a slower atomization process owing to a lower spray velocity [26]. Finally, this longer time to reach the steady-state regime at low P_{inj} (such as 400 bar) is more pronounced when a P_{amb} lower than 15 bar is used when compared to higher P_{inj}, based on the results of Li et al. [26].

It could be considered that the models of Payri et al. [11] and Katrašnik [12] are more complex as they require a momentum flux as input. In the absence of experimental data, one could consider using a simple mass flow rate model. Such models offer a good approximation of the variable needed in the prediction of fuel spray penetration and can easily be implemented as part of a design tool. Finally, considering the important role that multiple injection strategies play in reducing NO_x and soot emissions, it is important to also improve simple spray tip penetration models. One approach that might be worth investigating is based on the work of Zhou et al. [33] who concluded that the well-accepted linear time dependence of the spray tip penetration ($S_{tip} \propto t$) is not adequate for a proper prediction of the early part of the fuel spray tip penetration. Their conceptual model, obtained for long injections, divided the transient needle displacement in three consecutive periods, namely, the acceleration stage, the transition stage and the quasi-steady stage, each having a different exponent value associated with time. While the proposed model does not cover short injections and/or low P_{inj} as studied herein, the approach might help improve the prediction for such conditions. To do so, a high temporal resolution of the fuel spray tip measurement is needed to capture the early phase of the injection process.

Summary/Conclusions

The prediction of the fuel spray tip penetration is an important parameter in the design process of diesel engines. Considering the recent interest in using kerosene fuel in diesel engines, it was found necessary to evaluate how predicting models perform with this particular fuel. Therefore, experiments were conducted with a diesel injector fed with kerosene, and the fuel spray tip penetration and instantaneous mass flow rate were measured. Moreover, fuel spray tip penetration models with different complexities were briefly presented and compared to the experimental results. The main conclusions are summarized next.

The effects of injection conditions (P_{inj}, P_{amb} and ET) on the spray tip penetration were presented using the 'breakup scaling' method proposed by [27]. The non-dimensional results confirm the relationship $S^* = t^*$ before breakup ($t^* \leq 1$) and $S^* = \sqrt{t^*}$ after breakup ($t^* > 1$). The method was successfully applied with new fitted coefficients associated with the multi-hole injector and kerosene fuel tested herein.

It was observed that the models considered herein faced some difficulty predicting the early phase of the fuel spray penetration at a low injection pressure of 400 bar, even when a long injection duration of 2 ms was used. Better predictions were observed once the penetration reached the fully developed region.

Improvements in the predictions are observed, for all models, with increasing injection pressure, as the breakup time decreases in such cases. Once that breakup time is reached, the trend predicted by the models follow the experimental results when the injection duration is equal to or above 1 ms.

Short injections at injection pressures of 400 and 800 bar are difficult to predict with most models, with the exception of the model proposed by Katrašnik [12], which performed well for most conditions tested herein. The difficulty with the short injection duration is related to the fact that the models were initially developed for long injection durations. Finally, it is recommended that a simple spray penetration model be developed for short injection durations, given the importance of multiple injection strategies in diesel engine development.

References

[1] Lee, H., *Biodiesel, HSD, and JP-8 combustion process and emission characteristics in a dual-stage fuel injection condition.* International Journal of Energy and Power Engineering, 2014. **3**: p. 209.

[2] Lee, J., H. Oh, and C. Bae, *Combustion process of JP-8 and fossil Diesel fuel in a heavy duty diesel engine using two-color thermometry.* Fuel, 2012. **102**: p. 264-273.

[3] Ashour, M.K. and A.E. Elwardany, *Addition of two kerosene-based fuels to diesel–biodiesel fuel: Effect on combustion, performance and emissions characteristics of CI engine.* Fuel, 2020. **269**: p. 117473.

[4] Patil, K.R. and S.S. Thipse, *Characteristics of performance and emissions in a directinjection diesel engine fuelled with kerosene/diesel blends.* International Journal of Automotive and Mechanical Engineering, 2014. **10**: p. 2102-2111.

[5] Elsharkawy, E.A., et al., *Assessing and Comparing the Characteristics of CI Engine Powered by Biodiesel–Diesel and Biodiesel–Kerosene Blends.* Arabian Journal for Science and Engineering, 2021. **46**(12): p. 11771-11782.

[6] Chen, L., et al., *Comparative study of combustion and emissions of kerosene (RP-3), kerosene-pentanol blends and diesel in a compression ignition engine.* Applied Energy, 2017. **203**: p. 91-100.

[7] Yu, W., et al., *Macroscopic spray characteristics of kerosene and diesel based on two different piezoelectric and solenoid injectors.* Experimental Thermal and Fluid Science, 2016. **76**: p. 12-23.

[8] Song, L., et al., *Experimental study on spray characteristics of ethanol-aviation kerosene blended fuel with a high-pressure common rail injection system.* Journal of the Energy Institute, 2018. **91**(2): p. 203-213.

[9] Liu, L., et al., *A review of phenomenological spray penetration modeling for diesel engines with advanced injection strategy.* International Journal of Spray and Combustion Dynamics, 2020. **12**.

[10] Naber, J.D. and D.L. Siebers, *Effects of Gas Density and Vaporization on Penetration and Dispersion of Diesel Sprays*. 1996, SAE International.

[11] Payri, R., et al., *On the dependence of spray momentum flux in spray penetration: Momentum flux packets penetration model.* Journal of Mechanical Science and Technology, 2007. **21**(7): p. 1100-1111.

[12] Katrašnik, T., *Innovative 0D transient momentum based spray model for real-time simulations of CI engines.* Energy, 2016. **112**: p. 494-508.

[13] Hiroyasu, H. and M. Arai, *Structures of Fuel Sprays in Diesel Engines.* SAE Transactions, 1990. **99**: p. 1050-1061.

[14] Roisman, I.V., L. Araneo, and C. Tropea, *Effect of ambient pressure on penetration of a diesel spray.* International Journal of Multiphase Flow, 2007. **33**(8): p. 904-920.

[15] Bruno, T.J. and M.L. Huber, *Evaluation of the Physicochemical Authenticity of Aviation Kerosene Surrogate Mixtures. Part 2: Analysis and Prediction of Thermophysical Properties.* Energy & Fuels, 2010. **24**(8): p. 4277-4284.

[16] Liu, X., et al., *Direct injection of hydrogen main fuel and diesel pilot fuel in a retrofitted single-cylinder compression ignition engine.* International Journal of Hydrogen Energy, 2022. **47**(84): p. 35864-35876.

[17] Jourdain, C., J. Weiss, and P. Seers. *Comparison of image preprocessing methods for fuel droplet characterization*. in *47th AIAA Thermophysics Conference*. 2017.

[18] Li, M. and S. Ghosal, *Bayesian Multiscale Smoothing of Gaussian Noised Images.* Bayesian Analysis, 2014. **9**(3): p. 733-758.

[19] Chan, T.F. and L.A. Vese, *Active contours without edges.* IEEE Transactions on Image Processing, 2001. **10**(2): p. 266-277.

[20] Kim, J., J. Lee, and K. Kim, *Numerical study on the effects of fuel viscosity and density on the injection rate performance of a solenoid diesel injector based on AMESim.* Fuel, 2019. **256**: p. 115912.

[21] Manin, J., A. Kastengren, and R. Payri, *Understanding the Acoustic Oscillations Observed in the Injection Rate of a Common-Rail Direct Injection Diesel Injector.* Journal of Engineering for Gas Turbines and Power, 2012. **134**(12): p. 122801.

[22] Menucci, T., *Development of Bosch Rate of Injection Measurement Procedure and Results*. 2018, Michigan Technological University.

[23] Desantes, J.M., et al., *Experimental characterization of internal nozzle flow and diesel spray behavior. Part I: Nonevaporative conditions.* Atomization and sprays, 2005. **15**(5).

[24] Rajasegar, R. and A. Srna, *A Review of Current Understanding of the Underlying Physics Governing the Interaction, Ignition and Combustion Dynamics of Multiple-Injections in Diesel Engines.* SAE International Journal of Advances and Current Practices in Mobility, 2022. **5**(1): p. 117-134.

[25] Ross, S.M., *Peirce's criterion for the elimination of suspect experimental data.* Journal of engineering technology, 2003. **20**(2): p. 38-41.

[26] Li, Y. and H. Xu, *Experimental study of temporal evolution of initial stage diesel spray under varied conditions.* Fuel, 2016. **171**: p. 44-53.

[27] Arai, M. *Interpretative Review of Diesel Spray Penetration Normalized by Length and Time of Breakup (Similarity Law of Diesel Spray and Its Application)*. Energies, 2022. **15**.

[28] Zhou, X., et al., *Modeling diesel spray tip and tail penetrations after end-of-injection.* Fuel, 2019. **237**: p. 442-456.

[29] Das, S.K., K. Kim, and O. Lim, *Experimental study on non-vaporizing spray characteristics of biodiesel-blended gasoline fuel in a constant volume chamber.* Fuel Processing Technology, 2018. **178**: p. 322-335.

[30] Desantes, J.M., et al., *Development and validation of a theoretical model for diesel spray penetration.* Fuel, 2006. **85**(7): p. 910-917.

[31] Najar, I., et al., *Review of 1D Spray Tip Penetration Models and Fuel Properties Influence on Spray Penetration.* SAE International Journal of Engines, 2020. **13**(4): p. 521-544.

[32] Wang, Z., et al., *Experimental study on microscopic and macroscopic characteristics of diesel spray with split injection.* Fuel, 2016. **174**: p. 140-152.

[33] Zhou, X., T. Li, and P. Yi, *Modeling of diesel spray tip penetration during start-of-injection transients.* International Journal of Engine Research, 2020. **22**(9): p. 3013-3029.

Contact Information

Pierre-Lou Billerot (pierre-lou.billerot.1@ens.etsmtl.ca)

Acknowledgments

The financial supports of NSERC and CFI are greatly appreciated.

Definitions/Abbreviations

α	Gaussian shape factor
ΔP	Substantial injection pressure of the nozzle ($P_{inj} - P_{amb}$) [Pa]
$\Delta\rho$	Density difference ($\rho_f - \rho_{amb}$) [kg/m^3]
θ	Spray cone angle [°]
ρ_{amb}	Ambient air density [kg/m^3]
ρ_f	Fuel density [kg/m^3]
$\rho_{f,vap}$	Fuel vapor density [kg/m^3]
τ	Time constant in Roisman correlation (user-defined) [s]
$\mathcal{A}$	Bosch measuring tube section area [m^2]
a	Constant in Roisman correlation (user-defined) [m]
c	Speed of sound in ambient medium [m/s]
d_{equiv}	Equivalent diameter to the nozzle [m]
d_n	Nozzle diameter [m]
ET	Injection energizing time [s]
IMEP	Indicated mean effective pressure [kPa]
K_{bl}	Constant used in Equation (4) for breakup length [-]
K_{bt}	Constant used in Equations (3) and (12) for breakup timing [-]
K_u	Constant of proportionality between the spray axis velocity and the spray tip velocity used in Equation (6) [-]
L_b	Breakup length (noted R_0 in Equation (10)) [m]
$\dot{M}_0$	Instantaneous momentum flux [N]
$\widetilde{M}_0$	Time average momentum flux [N]
$\dot{M}_i$	Momentum flux of the ith packet in constant density model [N]
$\dot{m}$	Instantaneous mass flow rate [kg/s]
m_f	Fuel mass injected at time [kg]
m_{jet}	Total fuel mass injected [kg]
n_h	Number of holes of the injector [-]
$P(t)$	Dynamic pressure in Equation (1) [Pa]
P_{amb}	Ambient pressure [Pa]
P_{inj}	Injection pressure [Pa]
RPM	Revolutions per minutes [min^{-1}]
S	Fuel spray tip penetration [m]
S^*	Nondimensional fuel spray tip penetration [-]
S_i	Fuel spray tip penetration of the ith packet in constant density model [m]
S_{tail}	Spray tail penetration in variable density model [m]
T_{amb}	Ambient temperature [K]
t	Time [s]
t^*	Nondimensional time [-]
t_b	Breakup time [s]
t_i'	Scaled time after the injection of the ith packet constant density model [s]
U_{spray}	Spray tip velocity [m/s]